

Repelling Planet pairs by Ping-pong Scattering

YANQIN WU,¹ RENU MALHOTRA,² AND YORAM LITHWICK³

¹*Department of Astronomy & Astrophysics, University of Toronto*

²*Lunar and Planetary Laboratory, The University of Arizona*

³*Dept. of Physics and Astronomy, Northwestern University, 2145 Sheridan Rd., Evanston, IL 60208 & Center for Interdisciplinary Exploration and Research in Astrophysics (CIERA)*

ABSTRACT

The *Kepler* mission reveals a peculiar trough-peak feature in the orbital spacing of close-in planets near mean-motion resonances: a deficit and an excess that are a couple percent to the narrow, respectively wide, of the resonances. This feature has received two main classes of explanations, one involving eccentricity damping, the other scattering with small bodies. Here, we point out a few issues with the damping scenario, and study the scattering scenario in more detail. We elucidate why scattering small bodies tends to repel two planets. As the small bodies random-walk in energy and angular momentum space, they tend to absorb, fractionally, more energy than angular momentum. This, which we call "ping-pong repulsion", transports angular momentum from the inner to the outer planet and pushes the two planets apart. Such a process, even if ubiquitous, leaves identifiable marks only near first-order resonances: diverging pairs jump across the resonance quickly and produce the above asymmetry. To explain the observed positions of the trough-peaks, a total scattering mass of order a few percent of the planet masses is required. Moreover, if this mass is dominated by a handful of Mercury-sized bodies, one can also explain the planet eccentricities as inferred from transit-time-variations. Lastly, we suggest how these conditions may have naturally arisen during the late stages of planet formation.

1. INTRODUCTION

Orbital spacings between planets contain clues to their formation and evolution. This information is now abundantly provided by the thousands of multi-planet systems discovered by the *Kepler* mission. Most of exoplanets discovered by *Kepler* are Earth- to Neptune-sized with orbital periods up to about three years (limited by the lifetime of the *Kepler* mission).

The observed period spacings of neighboring planets have a broad distribution. At the lower end, the distribution appears to be sculpted by dynamical stability, in that spacings of period ratio less than about 1.3 are sparse. Above this, there is a broad peak that extends to period ratio about 2.5, and a long tail of larger spacings. Within this generally nondescript distribution, however, there exists one interesting feature. [Lissauer et al. \(2011\)](#); [Fabrycky et al. \(2014\)](#) reported a distinct excess of planet pairs just wide of, and a nearly empty gap just narrow of, certain first-order MMRs; Fig. 1 illustrates this trough-peak feature. According to [Steffen & Hwang \(2015\)](#), the statistically most significant amongst these are the large excess wide of the 3:2 MMR, and the clear deficit interior to the 2:1 MMR. These features lie about 1 – 2% away from exact resonance and have widths that are of the same magnitude. These val-

ues are a few times greater than the widths of these resonances (also marked in Fig. 1).

Much work has been expended in deciphering this precious feature. Theories where planets have undergone some degree of convergent migration predict clustering at the 2:1 and 3:2 MMRs, rather than the trough-peak feature. This disagreement could indicate either the absence of convergent migration, or a reorganization post-formation (see, e.g. [Izidoro et al. 2017](#); [Ghosh & Chatterjee 2023a](#)). There are two main categories of proposals to explain the trough-peak feature:

- repulsion by e-damping: damping of the orbital eccentricities (by friction with gas or planetesimals) leads to orbital divergence of a planet pair, akin to the spreading of an accretion disk when its energy (but not angular momentum) is removed by internal dissipation. This effect is strongly amplified near a MMR due to the larger forced eccentricities there, hence the term 'resonant repulsion' ([Lithwick & Wu 2012](#); [Batygin & Morbidelli 2013](#)). However, we argue below that updated data do not support this as the dominant mechanism.
- repulsion by scattering: [Chatterjee & Ford \(2015\)](#); [Ghosh & Chatterjee \(2023b\)](#) suggested that, in-

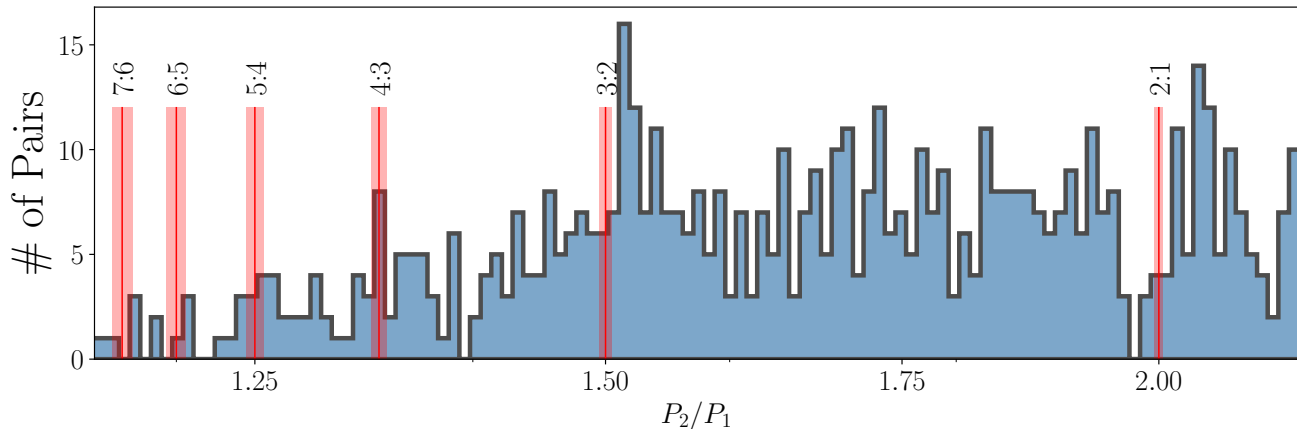


Figure 1. The observed distribution of period ratios for *Kepler* planet pairs. The colored lines mark both the centroids and the widths (estimated using eq. A2) of first-order mean-motion resonances.

stead of dissipation, scattering of planetesimals can also repel a planet pair and produce the observed feature. Although the repulsion effect is observed in their numerical simulations, there is no physical explanation. Moreover, the original proposals invoked massive planetesimal belts comparable in mass to those of the planets.

A few other explanations have also been proposed, including stochastic forcing by turbulence (Rein 2012), finite amplitude libration (Goldreich & Schlichting 2014; Xie 2014), and in situ planet mass growth (Petrovich et al. 2013). The first of these is hard to constrain or test, because the disk properties are not well known (see, e.g., Batygin & Adams 2017). The other two require planet-to-star mass ratios near that of Saturn/Sun, much larger than those in most of the *Kepler* systems, and thus fail to account for the magnitude of the observed asymmetry (e.g., see, §5 of Goldreich & Schlichting 2014).

We are motivated to revisit this issue now, a decade after much of the above works, because the past ten years have provided us with some more insights, both observational and theoretical. In particular, the following three considerations have persuaded us that the ‘damping’ proposal is not the main route.

First, to produce the observed asymmetry ($\sim 1\%$ in distance from a MMR) via damping, an extensive period of damping (over $100 \tau_e$, where τ_e is the e-damping time) is required (Lithwick & Wu 2012). One then expects all near-resonant pairs to have vanishingly small free eccentricities (eccentricities on top of that forced by planets). If so, all transit-time-variations (TTVs) should have transit phases pinned at some special values. This is not consistent with data (Fig. 2). Instead, TTV measurements returned free-eccentricities of order a couple percent (Lithwick et al. 2012; Wu & Lithwick

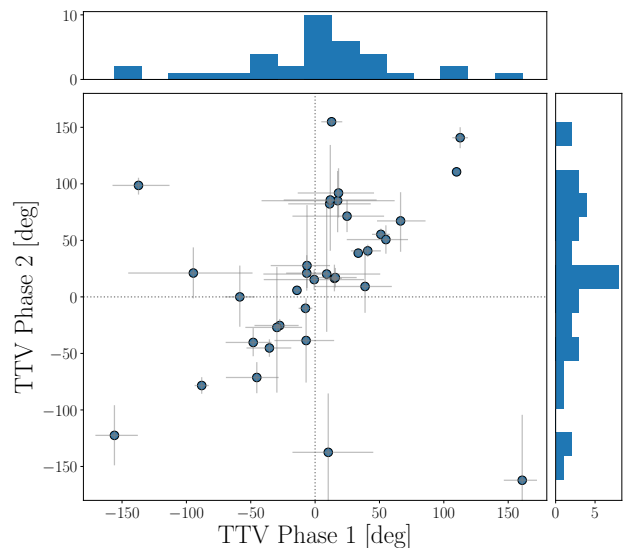


Figure 2. Transit-time-variations (TTV) reveal the non-zero free eccentricities in near-resonant planet pairs, inconsistent with the resonant repulsion. TTV phases (x-axis for the inner planets and y-axis for the outer) for 35 planet pairs around 3:2 and 2:1 MMRs are taken from Hadden & Lithwick (2014), but shifted by π from their convention for the outer ones. The error-bars indicate $1 - \sigma$ uncertainties. We have removed pairs with uncertainties greater than 60 deg, and the mean-error is now ~ 20 deg. The top and side panels show corresponding histograms for the phases. Pairs with zero free eccentricities should lie at the origin (0 deg, 0 deg). Observed pairs cluster around the origin but with a dispersion that is a few times larger than the mean error, indicating small but non-zero eccentricities.

2013; Hadden & Lithwick 2014, 2017). Choksi & Chiang (2022) attempted to remove this tension by invoking a third planet in the system that is eccentric. However, even though neighbouring companions are indeed quite commonly observed, its being eccentric will be surpris-

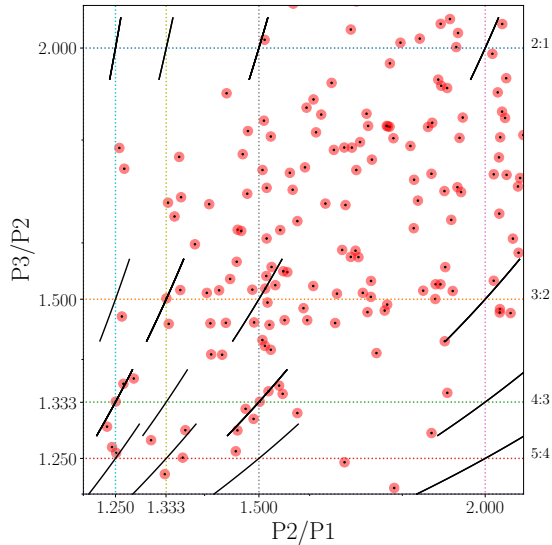


Figure 3. If eccentricity-damping is at work, one expects the period ratios of near-resonant triplets to obey the Laplace-like 3-body resonances (black curves, where $k_1 n_1 + k_2 n_2 + k_3 n_3 = 0$ and $k_1 + k_2 + k_3 = 0$, limited to $|k_1| + |k_2| + |k_3| \leq 12$). This does not seem overwhelmingly common.

ing – the extensive e-damping suffered by the planet pair would have to, somehow, spare the companion.¹

The same e-damping epoch would also have flattened the pairs down to co-planar orbits. However, while mutual inclinations in transiting systems are small, they are distinctly non-zero. [Fabrycky et al. \(2014\)](#) estimated an inclination dispersion of 1 – 2 deg, based on the impact parameters. For systems with high-multiple transiting planets, [Zhu et al. \(2018\)](#) inferred a somewhat smaller value of ~ 0.8 deg.

Lastly, the triplet structure appear inconsistent with extensive e-damping. [Batygin & Morbidelli \(2013\)](#) considered a chain of 3 planets subject to e-damping and found that they should be deposited along the so-called Laplace-like 3-body resonances ($k_1 n_1 + k_2 n_2 + k_3 n_3 = 0$, with $k_1 + k_2 + k_3 = 0$ and n_i the mean-motions). With such a combination of orbital periods, forced eccentricities on the middle planet from its two neighbours cancel effectively, because the they have the same forcing periods but opposite phases. So these ‘three body resonances’, different from the usual mean-motion resonances, minimize the forced eccentricities. However, such a preference does not seem overwhelmingly common in known triplets ([Pichierri et al. 2019](#), also see

¹ Giant companions at larger separations, an uncommon occurrence, may be more plausible for this scenario.

[Fig. 3](#) here), though a more thorough statistical study on the degree of prevalence is merited

These failures of the e-damping proposal motivate us to take a deeper look at the ‘scattering’ proposal. We would like to understand the physical reason why scattering leads to orbital repulsion, to assess the amount of scattering mass required to produce the observed asymmetry, and to determine whether the scattering process can self-consistently explain the observed free eccentricities and free inclinations.

In this work, we use the term “ping-pong repulsion” to refer to the process in which planetesimals (“ping-pongs”) scatter off of a pair of planets and cause the planets to repel each other. We explain the underlying cause for repulsion (§2), and clarify the conditions required to explain the observed asymmetry (§3). We end by suggesting a plausible scenario where these conditions naturally arise, as well as other extant issues (§4).

2. PING-PONG REPULSION DISSECTED

It is known that planets can undergo divergent migration when scattering planetesimals. For example, Jupiter can eject bodies that are sent inward by Neptune, so Jupiter loses energy while Neptune gains ([Fernandez & Ip 1984](#); [Hahn & Malhotra 1999](#)). This well-known mechanism is, however, different from our problem here. One significant difference is that Jupiter easily ejects bodies from the Solar System because its surface escape speed exceeds its orbital speed.

By contrast, *Kepler* planets are in the opposite limit. They lie so deeply in their stars’ gravitational potential well, they cannot easily eject bodies. Instead, they relentlessly scatter the planetesimals until physical collision and merger occur. In this case, do the orbits of a pair of scattering planets pull apart or converge?

2.1. Ping-pongs repel a pair

Numerical experiments often show that, when the planets scatter small bodies, divergent migration takes place ([Chatterjee & Ford 2015](#); [Morrison & Kratter 2018](#); [Ghosh & Chatterjee 2023b](#)). Here we demonstrate this effect and provide a physical explanation for the repulsion: an uneven phase space.

Consider first the numerical example of one ping-pong ([Fig. 4](#)). It is in an initially nearly circular ($e = 0.05$), nearly co-planar orbit between two circular, co-planar planets (the inner planet at 0.1au). It is excited into orbit crossing with the planets by dynamical instability.² Subsequent close-encounters force the ping-pong to random-walk in energy and angular momentum space,

² A more circular ping-pong may sometimes not reach this state.

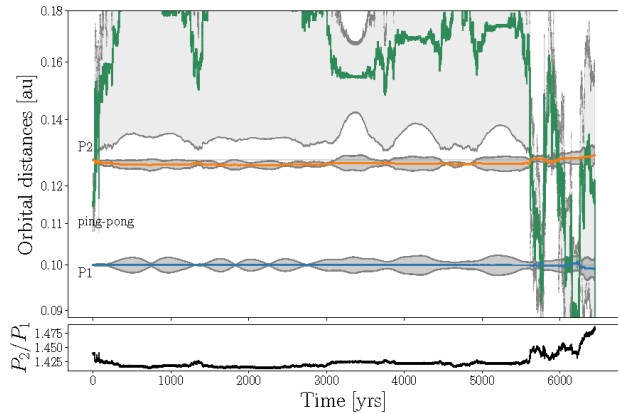


Figure 4. A pair of planets scattering and finally accreting a ping-pong. The planets are each $8M_{\oplus}$, and the ping-pong is 1.3% of the combined planet mass. The top panel shows the semi-major axis, apoapse, and periapse for each body. The bottom panel shows the planets’ period ratio, which increases by $\sim 3\%$ by the time the ping-pong is accreted. The final accretion has little effect on the period ratio.

until it is accreted by one of the planets. Even though the ping-pong gains or loses energy with roughly equal probability during each encounter, by the time of the merger, the ping-pong has successfully transferred energy and angular momentum from the inner to the outer planet and pushed them apart. Such an outcome appears common among most simulations.

We numerically integrate the system using the REBOUND code (Rein & Liu 2012) with the IAS15 integrator (Rein & Spiegel 2015) at a minimum timestep of 10^{-10} day. Masses for the planets and the ping-pong are M_p ($= M_{p1} = M_{p2}$) and m , respectively. Here we take $M_p = 8M_{\oplus}$ and $m = 1.3\% \times (M_{p1} + M_{p2}) \approx 4$ Mercury masses. We assume the ping-pong has a negligible radius ($R = 0$), while the planets have radii $R_p = 1.5R_{\oplus}$. The merger occurs after a few thousand years and is modelled as conserving linear momentum but dissipating all relative motion.

To understand this average fate of repulsion, we turn to concepts like Jacobi integral and phase space. When the ping-pong interacts with a single planet, it very nearly conserves its Jacobi constant relative to that planet³

$$\text{Jacobi} = \sqrt{a}(1 - u) + \frac{n\sqrt{a}}{2n_p} \quad (1)$$

³ The conservation of Jacobi constant is violated by a correction that is $O(m^2/M_p^2)$. Note that our definition of the Jacobi constant differs from the usual one by an unimportant overall constant.

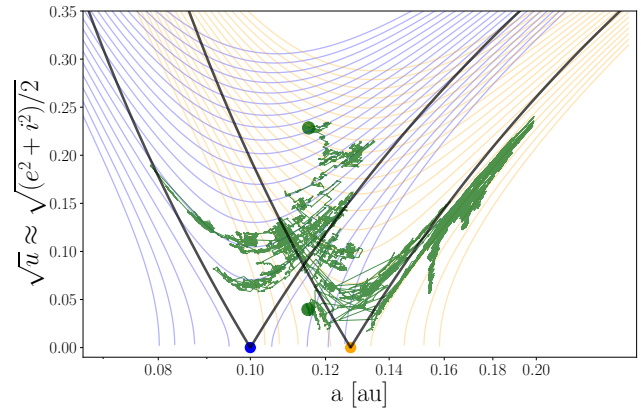


Figure 5. Ping-pong dynamics in the $a-\sqrt{u}$ plane, where u is random motion. The green jagged trajectory traces the ping-pong from Fig. 4, with its initial and final states shown as the lower and upper green circles. The blue and orange circles represent the planets. Each planet’s curves of constant Jacobi integral are shown with its corresponding color. The ping-pong’s trajectory alternates between tracking the blue and orange curves, as it diffuses upwards. The black curves show the regions within which the ping-pong can cross a planet’s orbit (for $i = 0$).

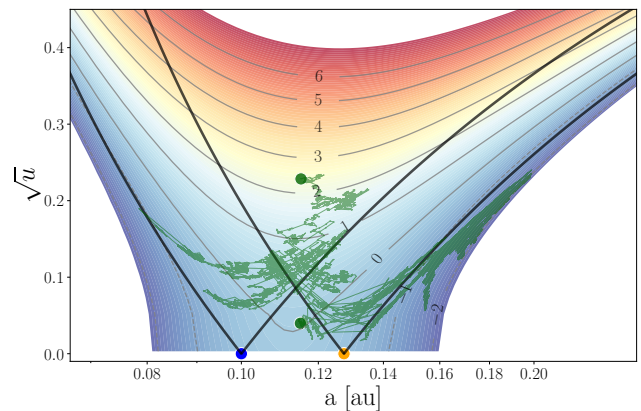


Figure 6. Origin of the repulsion. Again for the case in Figs. 4-5. Here, instead of the Jacobi curves, the background colours and contours indicate the amount of planet repulsion ($\Delta(P_2/P_1)$), measured in unit of $\epsilon = m/(M_{p1} + M_{p2})$, as the ping-pong random walks in the $a-u$ space. Most of the phase space that the ping-pong can access leads to repulsion. Orbital change due to ping-pong accretion is not included here.

where $n = \sqrt{GM_*}a^{-3/2}$ is the ping-pong’s mean-motion, n_p that for the planet, and

$$u \equiv 1 - \sqrt{1 - e^2} \cos i \approx (e^2 + i^2)/2, \quad (2)$$

is related to the angular-momentum-deficit (AMD, Laskar 1997) via $\text{AMD} = m\sqrt{a}u$. Curves of constant Jacobi values, for individual planets, are plotted in Fig. 5. At any given time, the ping-pong chiefly interacts with,

and evolves along a curve of constant Jacobi with respect to, that planet. But when it switches its main scatterer, the ping-pong can switch Jacobi curves. This switching-over allows the ping-pong to random-walk through a large phase space. Over time, the ping-pong appears to climb the Jacobi ladder to ever higher values of u because the phase space volume at high eccentricity and high inclination is larger.

Fig. 6 presents the consequences of such a random-walk: repulsion. Regardless of the ping-pong's mass, the following conservation of total energy and angular momentum apply before the merger event,

$$\sum_{i=1}^2 \frac{M_{pi}}{a_i} + \frac{m}{a} = \text{const},$$

$$\sum_{i=1}^2 M_{pi} \sqrt{a_i} (1 - u_i) + m \sqrt{a} (1 - u) = \text{const}. \quad (3)$$

If we simplify by setting $u_1 = u_2 = 0$, we can predict the change in planet spacing (measured as changes in the period ratio, $\Delta(P_2/P_1)$) as a function of (a, u) . This is shown by the colour contours in Fig. 6. As the ping-pong climbs the Jacobi ladder, it tends to increase in u (angular momentum deficit). So fractionally speaking, it removes more energy than angular momentum from the planet duo. This repels the pair, increasing in degree as the ping-pong diffuses to higher values of u . There is an analogy of this physics in an accretion disk: as kinetic energy is converted into heat by, e.g., turbulence, the conservation of angular momentum dictate that the disk must spread radially. Another analogy, less accurate, is when a real ping-pong push apart two paddles as it scatters off of them.

In summary, driven by the urge to explore more phase space, the ping-pong on average repels the planet pair.

In the meantime, the scatterings also affect the eccentricities and inclinations of the planets. This can be thought of as a process of AMD equipartition (Wetherill & Stewart 1989). This yields, to order of magnitude, $e_p \sim \sqrt{m/M_p} e$, and inclinations that are about half the eccentricities (see Kokubo & Ida 1998, and Fig. 9 here).

2.2. Accretion and the Average Repulsion

The planets have finite sizes, so the ping-pong will be accreted after a time. This has two effects: it truncates the time for the ping-pong to transfer energy; second, the inelastic collision modifies the planetary orbit.

The accretion time, for an orbit-crossing ping-pong, is (ignoring gravitational focussing),

$$t_{\text{merger}} \sim \frac{1}{4} P_{\text{orb}} \times \frac{2\pi a^2}{\pi R_p^2} \sim 4 \times 10^4 \text{yrs} \left(\frac{a}{0.1 \text{au}} \right)^{3.5} \left(\frac{R_p}{1.5 R_{\oplus}} \right)^{-2}. \quad (4)$$

This estimate is confirmed by numerical simulations (Fig. 7), with the caveat that gravitational focussing may be important early-on, before the ping-pong is dynamically excited.

A ping-pong that survives longer can diffuse to higher u (AMD) and can cause more repulsion. As this is a stochastic process, we gauge the average amount of repulsion by simulating the ping-pong with randomized initial phases (Fig. 4). Summing over these results, we find an average repulsion of

$$\Delta \left(\frac{P_2}{P_1} \right) \equiv \left(\frac{P_2}{P_1} \right)_{\text{final}} - \left(\frac{P_2}{P_1} \right)_{\text{init}} \approx 1.1 \times \frac{m}{M_{p1} + M_{p2}} = 1.1 \times \epsilon, \quad (5)$$

where ϵ is the fractional mass of the ping-pong. This is also the result one obtains if the single ping-pong is split into an infinite number each with an infinitesimal mass, so we call this result the 'continuum limit'. The factor 1.1 is valid for our set of parameters, i.e., near 3:2 MMR,⁴ and with our assumed accretion cross-section. If the planets have larger accretion cross sections, the survival time is shorter and the repulsion will be correspondingly smaller.

The mergers themselves typically cause negligible changes to the planet spacing. Consider a planet on a circular orbit that merges with a ping-pong. The change in the planet's semi-major axis (δa_p) is given by the change in its specific energy, or $\delta a_p/a_p \approx \frac{2m}{M_p} \mathbf{V} \cdot \Delta \mathbf{v}/v^2$, where \mathbf{V} is the planet's initial (circular) velocity, and $\Delta \mathbf{v}$ is the ping-pong's pre-collision velocity relative to the planet. Taking the guiding center approximation, the magnitude $|\Delta \mathbf{v}|/V \sim e$, where e is the ping-pong's pre-collision eccentricity. Therefore every time a ping-pong merges with the planet, it changes the planet's a_p by $|\delta a_p/a_p| \sim (m/M_p) e \sim \epsilon e$. This is smaller than that in eq. (5) by a factor of e . In addition, this change has random signs, because the angle between $\Delta \mathbf{v}$ and \mathbf{V} is random. So we can typically ignore this effect.

2.3. Boost when Crossing a Resonance

The above picture of gradual repulsion is modified when the planet pair encounters a first-order MMR. At the resonance separatrix, a rapid and coherent energy and angular momentum transfer between the pair ensues. The pair pushes each other apart quickly, on the timescale of resonance libration.

The dynamics of a divergent resonance crossing is summarized in Appendix A. The amount of repulsion

⁴ The value is slightly less for 2:1 MMR.

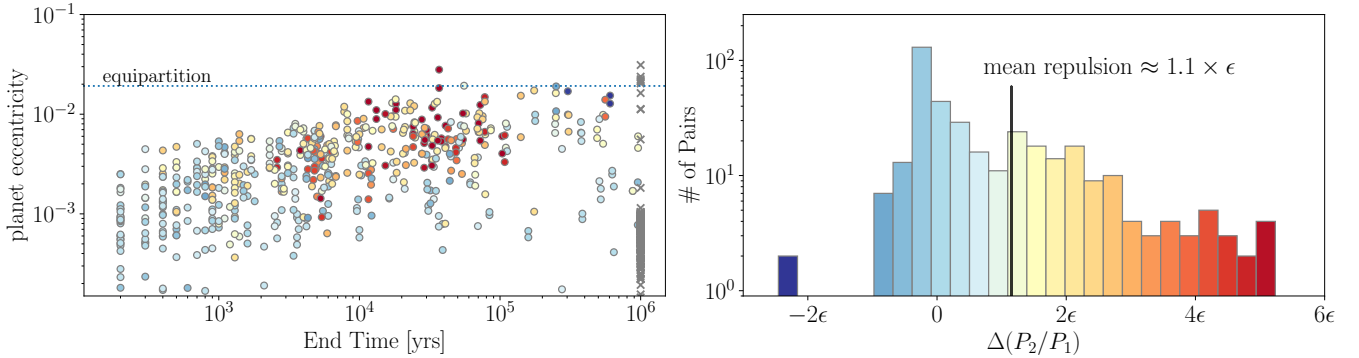


Figure 7. Ensemble results from 1000 simulations that are identical to Fig. 4, except with randomized initial orbital phases for the ping-pong. The left panel shows the final planet e vs. time of merger. The right panel shows the histogram for the net amount of pushing, for the ensemble. The color code in both panels quantifies the amount of repulsion. The left panel also shows that in systems where the ping-pong lives longer, the planets approach closer to equipartition eccentricity ($\sim (m/M_p)^{1/2} e$, the dotted line evaluates for $e = 0.3$). Around 1/3 of the systems (marked as gray crosses) remain in limbo even after the integration limit of 10^6 yrs. They are discarded from the analysis.

contributed by the 3:2 MMR is,

$$\Delta \left(\frac{P_2}{P_1} \right)_{3:2\text{MMR}} \approx 0.0095 \left(\frac{M_p}{8M_\oplus} \right)^{2/3} \quad (6)$$

for equal-mass planets. For the 2:1 resonance, the numerical coefficient is instead 0.0083. Appendix A also provides an estimate for the associated eccentricity kick. We illustrate these results in Fig. 12, where we numerically simulate a pair of planets gently pushed apart to cross the 3:2MMR.

This resonance boost accelerates the repulsion at the MMR. It leads naturally to a deficit of pairs to the narrow of the MMR, and to an excess to the wide. Together with the ordinary repulsion (eq. 5), one can then account quantitatively for the *Kepler* asymmetry.

3. RESULTS

Here, we will simulate a large number of systems, varying parameters like ping-pong masses and numbers, and compare the results against observed pairs. For brevity, we focus on planet pairs near the 3:2 MMR.

3.1. Simulations

We continue to adopt the same planet parameters as before: $M_{p1} = M_{p2} = 8M_\oplus$; planet radii $R_p = 1.5R_\oplus$; initially circular and co-planar orbits with the inner one at $a_{p1} = 0.1\text{au}$. We place the outer planet near the 3:2MMR, with an instantaneous period ratio that is flatly distributed from 1.40 to 1.60. The word ‘instantaneous’ is only relevant within the libration width of an MMR.

The planetesimals (ping-pongs) are placed randomly from $a_{p1}/1.2$ to $1.2 \times a_{p2}$. Bodies in this range are found by Ghosh & Chatterjee (2023b) to be actively interacting with the planets (their Fig. A1). The initial eccentricities and inclinations of these bodies are assumed

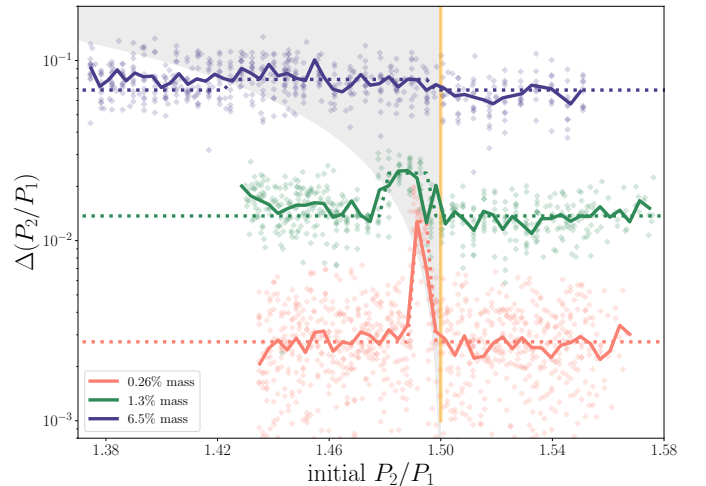


Figure 8. Repulsion of planet pairs, as a function of their initial period ratio (see Fig. 9 for the final one). Each group of colored points represent simulations with the same total mass (ϵ) but a variety of ping-pong numbers (N). The thick colored lines depict the local mean, showing that the repulsion only depends on ϵ . Points inside the shaded region encounter the 3:2MMR and therefore receive a resonance boost (eq. 6). Together, the repulsion is well described by the dotted lines, which are the sum of eq. (5) and eq. (6).

to follow Rayleigh distributions with modes 0.05 and $0.05/2$, respectively.⁵ We choose a total mass for the ping-pongs (mass ratio $\epsilon \equiv m/(M_{p1} + M_{p2})$, with ϵ ranging from 0.26% to 6.5%) and spread the mass among N particles (ranging from 5 to 200). We expect the total mass to be the most important variable, with the value of N only affecting the dispersion. We ignore mutual

⁵ Dynamically cooler ping-pongs are harder to excite to planet crossing orbits. But it may only be a matter of time in a tightly packed planetary system.

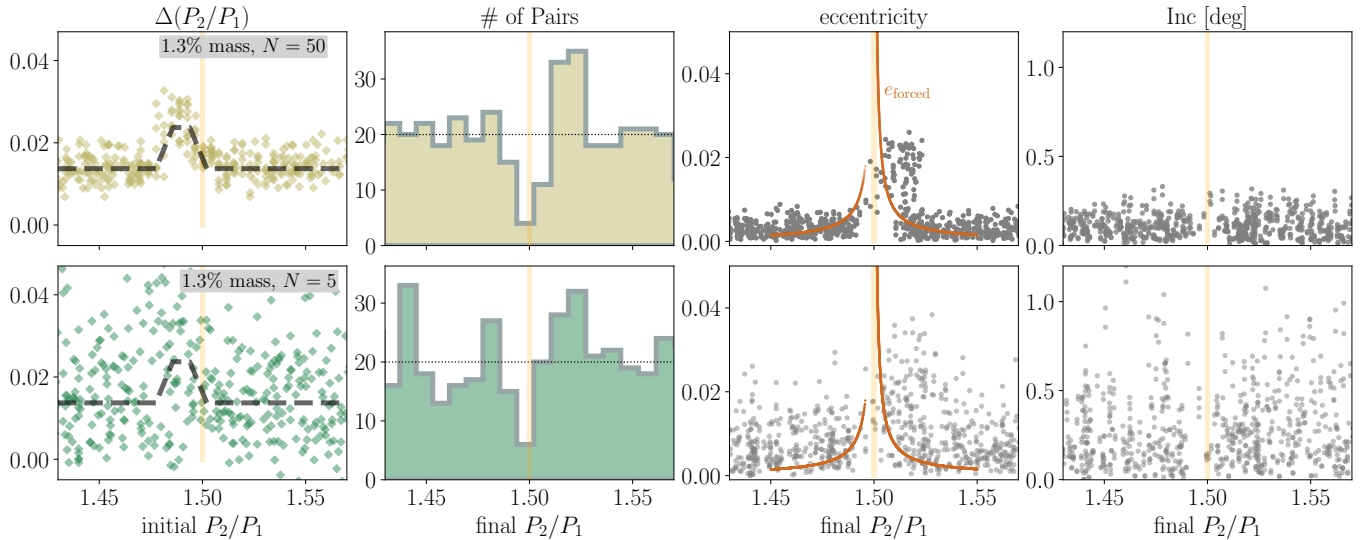


Figure 9. Comparing detailed simulation results using light (top) and heavy (bottom) ping-pongs, for the same total mass of $\epsilon = 1.3\%$. Each ping-pong in the top panel weighs 0.08 that of Mercury, while those in the bottom weighs 0.8 Mercury. The left-most panels show the amount of repulsion, with the thick dashed lines indicating the so-called ‘continuum limit’ (eq. 5-6). The left-middle panels show the initial (dotted lines) and final (colored histogram) distributions in P_2/P_1 . The bottom group exhibits a larger poisson noise, translating into a more jagged period distribution, and a less well-defined resonance asymmetry. The panels to the right show the final planet eccentricities and inclinations. Planets in the upper group are only weakly excited, with eccentricity kicks from resonance crossing clearly visible. In contrast, the bottom group are excited to values that, if described by Rayleigh distributions, have modes of $\sigma_e \sim 0.008$ and $\sigma_{\text{inc}} \sim \sigma_e/2 \sim 0.004$ radian (or 0.25 deg).

collisions between the ping-pongs by setting their physical sizes to zero. Moreover, the ping-pongs are taken to be pseudo-test particles, namely, they exert force on the planets but not amongst themselves. We integrate the system until all ping-pongs have been accreted, or when we reach 10^6 yrs.

Fig. 8 shows the collected results. All planet pairs experience repulsion, with a magnitude of $\sim \epsilon$ (eq. 5). Pairs that encounter a first-order MMR during the process experience an additional boost that is of order the resonance width (eq. A2). As ϵ increases, more pairs to the narrow of MMR can encounter the MMR and enjoy this boost.

To further illustrate some details, Fig. 9 compares two simulations of the same total mass (ϵ) but different N . The run with a smaller N (more massive ping-pongs) exhibit more scatter, translating into a more subdued resonance asymmetry and an overall more jagged period distribution. The effects of N are also seen in the final values for planet eccentricity and inclination. These quantities diffuse with time to near equipartition values ($\sim \sqrt{m/M_p e}$), after a time comparable to the merger time. The simulation with heavier ping-pongs (Mercury-mass) produces an eccentricity excitation that can be described by a Rayleigh distribution with a mode of $\sigma_e = 0.008$, while the lighter group produces one that is ~ 3 times smaller. In addition, the planets receive

eccentricity kicks when they cross a resonance (see Appendix).

3.2. Explaining the Data

Fig. 10 shows the observed and the computed asymmetries around the 3:2MMR. The excess to the wide of the resonance is situated around $P_2/P_1 \sim 1.52$, and is best reproduced with a total ping-pong mass of $\epsilon \sim 1\%$. A similar conclusion is reached to explain the pairs near the 2:1 MMR. In the same figure, we also contrast the scattering scenario against the damping scenario. Using the formulation from Lithwick & Wu (2012), one finds that an extensive period of eccentricity damping, of order 10^3 e-damping times, is required to reproduce the same asymmetry (see §1).

Observationally, both the 3:2 and 2:1MMRs show an excess of pairs to the wide of the resonances, but only the 2:1 shows a clear deficit to the narrow (Fig. 1). We will discuss this issue in §4.5.

Now we turn to consider planet eccentricities. Hadden & Lithwick (2014) reported, for a sample of 54 planet pairs, a Rayleigh mode of $\sigma_e = 0.018$. This is a couple times larger than that in our simulations with Mercury-mass ping-pongs. These eccentricities are derived from the observed TTV phases (see §1), so a more direct comparison should be done in terms of TTV phases. The data in Fig. 2 consists of 35 pairs, which are the better measured subset out of the 54 pairs in Hadden & Lith-

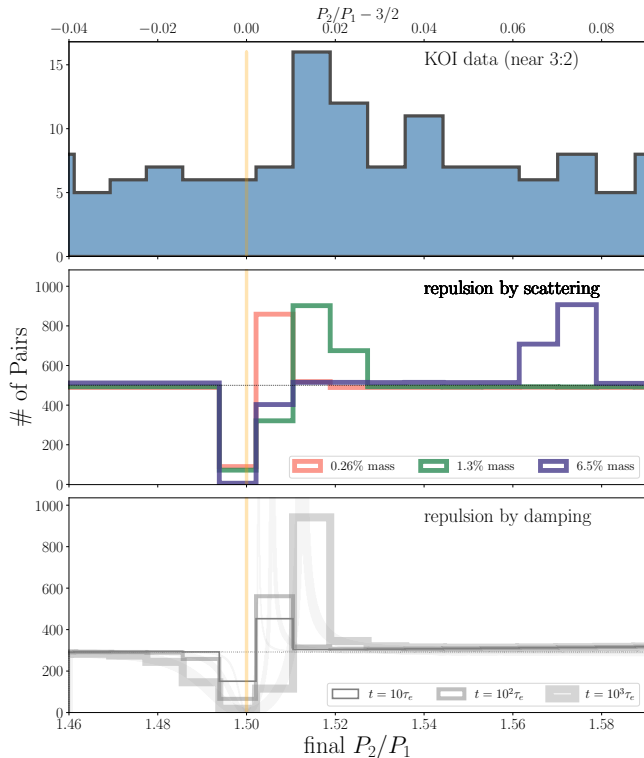


Figure 10. Resonance asymmetry near the 3:2MMR, observed (top panel) versus predicted (two lower ones, with the thin dotted lines indicate the initial distribution of period ratio). The middle panel shows the results of repulsion by scattering, for different values of ϵ (fractional mass in the planetesimals) and evaluated in the so-called ‘continuum limit’ (eq. 5-6). The lower panel depicts repulsion by e-damping (Lithwick & Wu 2012), for different damping durations (measured in e-damping times), and in both histogrammed and unhistogrammed forms.

wick (2014). We compare these against those from our simulated pairs from Fig. 9. For the latter, we extract TTV information as follows. For each planet, we express its transit times as the sum of four terms: a linear trend, an offset, and two sinusoidal terms that account for the amplitude and phase of the TTV (Eq. 18 in Lithwick et al. 2012). The four coefficients of these terms are extracted via linear least-squares (Press et al. 1986). We then convolve the simulated TTV phases with a measurement error of 20 deg and compare the distributions in Fig. 11. We find that only the simulations with heavier ping-pongs (Mercury-mass) can explain the observed spread in the TTV phases.

The heavy ping-pong run also yields planet mutual inclinations that are nearly Rayleigh with a mode of 0.25 deg. This value is a few times smaller than the 0.8 deg inferred for the high-multiple systems (Zhu et al. 2018), and a larger factor away from the 1 – 2 deg inferred for general pairs (Fabrycky et al. 2014). We con-

sider this a partial success of our theory: the ping-pongs can impart some non-coplanarities to the planets, and it is possible that further dynamical instabilities, not captured in our theory, have set in to increase the dispersion.

In summary, our simulations suggest that a handful of Mercury-mass ping-pongs can explain the resonance asymmetry, the magnitudes of the free eccentricities, and partially, the mutual inclinations.

4. DISCUSSION

We propose that ping-pong repulsion is responsible for the observed MMR asymmetry. Repulsion should have occurred across all pairs, not just those close to an MMR. But its effect is clearly discernible only near an MMR.

In the following, we provide an astrophysical context that may give rise to such a universal behaviour (§4.1). We will also consider how the dynamics changes when the planets have gaseous envelopes (§4.2). In §4.3, we point out that accretion is likely complicated. We discuss previous works in §4.4, and an important caveat in §4.5.

4.1. A plausible story

Our calculations suggest the presence of a handful of Mercury-mass objects (radius $R \sim 2300$ km if at Earth composition) that make up $\sim 1\%$ of the planet masses, at late stages of planet formation. What astrophysical context can naturally give rise to this population of bodies?

The following estimate is thought-provoking. We have ignored ping-pong mutual collisions in previous sections. But they do collide. Orbit-crossing ping-pongs should collide with each other at a timescale

$$t_{\text{coll}} \sim 3 \times 10^5 \text{ yrs} \left(\frac{a}{0.1 \text{ au}} \right)^{3.5} \left(\frac{\epsilon}{1\%} \right)^{-1} \left(\frac{R}{2300 \text{ km}} \right). \quad (7)$$

Within uncertainties, this is comparable to the planet accretion time of ping-pongs, $t_{\text{merger}} \sim 4 \times 10^4$ yrs (eq. 4). Is this a coincidence?

Let us first imagine a situation where $t_{\text{coll}} \ll t_{\text{merger}}$, i.e., ping-pongs are small and collide frequently with each other. This may introduce collisional cooling to their orbits, grind them down to smaller debris, and in general forestall orbit-crossings with the planets. Only when the ping-pongs grow large enough so that $t_{\text{coll}} \sim t_{\text{merger}}$, can the scattering/accretion proceed.

Let us now consider the opposite limit when the mass is dominated by too few large ping-pongs and $t_{\text{coll}} \gg t_{\text{merger}}$. These will be quickly accreted but the accretion process is messy (see §4.5): grazing impacts and tidal

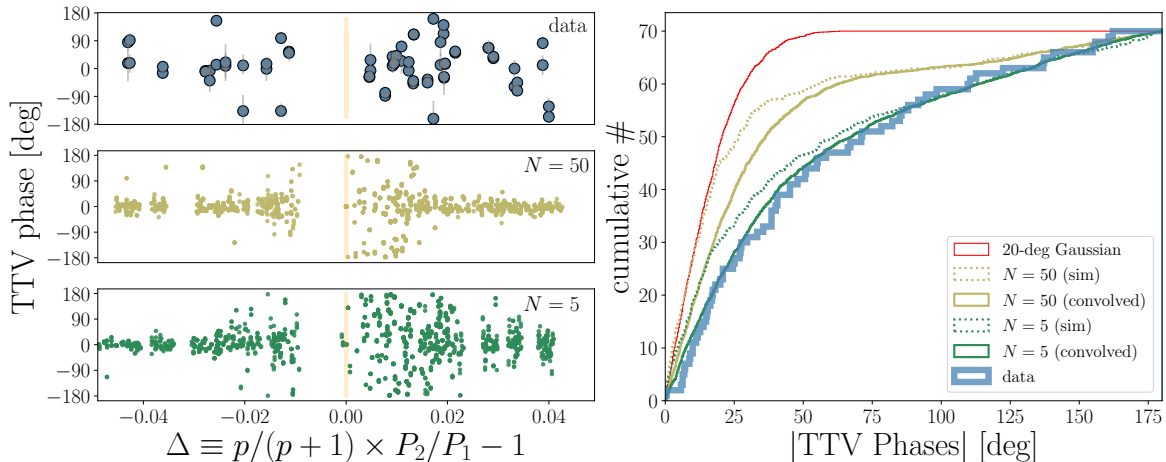


Figure 11. Comparing TTV phases between data and simulations. For the observed values, we take the same 35 pairs from Fig. 2 and express their period ratios as $\Delta = p/(p+1) P_2/P_1 - 1$ to capture their respective MMRs. The simulations are the two sets from Fig. 9. The left panels compare how the TTV phase depend on the distance to the MMR, and the right compares the cumulative distributions of the TTV phases. Here, the red curve describes a population with zero free-eccentricities (convolved with the typical noise, a Gaussian of 20 deg), and represents the prediction from repulsion by e-damping. The simulation with heavy ping-pongs, after convolving with the same Gaussian, agrees well with the observed TTV phase distributions (p-value 0.9). The lighter ping-pong model, on the other hand, has a p-value of 0.0015. This suggests that individual planetesimals should have \sim Mercury mass.

disruptions may allow some of the ping-pong mass to escape in the form of small fragments. These fragments may be in the collisional regime ($t_{\text{coll}} \ll t_{\text{merger}}$) and the previous discussion applies.

As a result, one can imagine that, when ϵ drops from unity to zero over many decades, the dominant ping-pongs continuously evolve in size to maintain $t_{\text{coll}} \sim t_{\text{merger}}$, or a ping-pong size $R \propto \epsilon$, and a ping-pong number, $N \propto R^{-2} \propto \epsilon^{-2}$. For our parameters, $N \sim 5 \times (\epsilon/1\%)^{-2}$.

In such a picture, $\epsilon \sim 1\%$ is special. First, this makes the resultant MMR asymmetry clearly visible – a smaller ϵ would produce too weak a repulsion and very few pairs can be pushed towards and jump across the resonance (see the case with the lowest ϵ in Fig. 10). Second, the asymmetry signature is less stochastic at this value of ϵ because $N \sim 5 \gg 1$ – at a much larger value of ϵ , ping-pongs will be fewer in number ($N \ll 5$) and almost planet-like in size. They would cause large repulsion but the signature is too stochastic to be recognizable (compare the two rows in Fig. 9). In fact, ping-pong repulsion in this stage may give rise to a nearly flat period distribution, as observed in generic planet pairs; it can also leave a finger-print in the eccentricity/inclination excitations.

So in conclusion, we suggest that the late stage of planet formation is a time of clearing of a substantial amount of debris. The ping-pong generation with $\epsilon \sim 1\%$ leaves the last and the clearest MMR signature, explaining naturally the observed asymmetry at

1 – 2% away from exact MMR. More massive early generations may instead account for the nearly feature-less pair spacing in *Kepler* planets.

4.2. Gas: accretion and erosion

Many of the *Kepler* planets possess low-mass hydrogen envelopes (mass of order 1%), the so-called mini-Neptunes. It is likely that they accrete these envelopes before the gas disks disperse.

In the following, we consider how the presence of a gaseous envelope affects ping-pong accretion, and, importantly, whether the ping-pongs can strip the planets of their envelopes. This discussion assumes that the scattering occurs after gas accretion. This is possible, despite the fact that the disk lifetime (Myrs) is much longer than the time to clear the ping-pongs (eq. 4). For instance, dynamical friction (either from gas or from mutual collisions) may place the ping-pongs into psuedo-stable orbits (like the gray crosses in Fig. 7), so they may reside there for millions of years before being dislodged by weak perturbations.

4.2.1. Gas Envelope and Accretion

Previously, we have set the planet’s accretion radius to be its core size. Now we consider mini-Neptunes. The observed hydrogen atmospheres contain about a percent of the planets’ masses, but expand their physical sizes by a factor of 2. The mean density of the atmosphere is then smaller than the solid (core) density, by a factor of $\rho_{\text{atm}}/\rho_{\text{solid}} \sim 10^{-3}$. A solid planetesimal travelling through the atmosphere will lose a fraction of its energy

that is roughly the ratio of the encountered mass to its own mass,

$$\frac{\delta E}{E} \sim \frac{\rho_{\text{atm}}}{\rho_{\text{solid}}} \times \left(\frac{R_p}{R}\right) \sim \left(\frac{25 \text{ km}}{R}\right), \quad (8)$$

with merger occurring whenever $\delta E/E \sim 1$. So for our preferred ping-pongs (Mercury-mass, $R \sim 2300 \text{ km}$), the atmosphere presents little ability to capture. This justifies our using the super-earth size for merger.

4.2.2. Survival of the Gas Envelope

Would the ping-pongs remove the gas envelopes? This is a relevant point because the ping-pong mass fraction ($\epsilon \sim 1\%$) is comparable to the envelope mass fraction of the mini-Neptunes.

Let us first consider a grazing impact where the ping-pong misses the solid core. The encounter speed is very supersonic, so the ping-pong simply punches a hole in the atmosphere, carrying away with it the fraction of the envelope that is in its path, or of order $(R/R_p)^2 \sim 1\%$ of the envelope mass, with R_p taken to be $4R_\oplus$. Multiple impacts may enhance this fraction, but the ping-pong will likely experience an impact that hits the solid core and be absorbed, before it is able to strip off the envelope.

For ping-pongs that hit the solid core, a shock emerges at the antipole of the impact point, accelerating the gas there to escape. According to Yalinewich & Schlichting (2019) and their corrected results (Yalinewich & Schlichting 2020), even for an impact speed that is twice the surface escape ($\sim 25 \text{ km/s}$ for our super-Earths) and an impactor that is $\sim 1/4$ in radius to the target, only about 10^{-3} of the envelope can be removed. This is immaterial.

4.3. Messiness of the Accretion Process

The process of merger with a solid core, on the other hand, can be a messy business.

For one, tidal disruption, as opposed to a complete accretion, may interfere. While the ping-pong density can be terrestrial (we take $\rho_p = 5 \text{ g/cm}^3$), that of the super-Earth is higher due to gravity compression, and can be $\rho_{\text{core}} = 12 \text{ g/cm}^3$ (corresponding to $8M_\oplus$ and $1.5R_\oplus$). This enhances the cross-section for complete tidal disruption over that for accretion. For instance, for a high velocity impact of $v_\infty = 0.5v_{\text{esc}}$ (this corresponds to $e \sim 0.15$), Boss et al. (1991); Watanabe & Miyama (1992) predict a destruction distance of,

$$\begin{aligned} R_{\text{Roche}} &\sim 1.0R_{\text{core}} \times \left(\frac{\rho_{\text{core}}}{\rho_p}\right)^{1/3} \\ &\sim 1.3R_{\text{core}} \left(\frac{\rho_p}{5 \text{ g/cm}^3}\right)^{-1/3} \left(\frac{\rho_{\text{core}}}{12 \text{ g/cm}^3}\right)^{1/3} \end{aligned} \quad (9)$$

This distance expands further by a factor of 1.7 if the encounter is parabolic (Sridhar & Tremaine 1992; Watanabe & Miyama 1992). Tidal disruption can return a fair fraction of the ping-pong mass to stello-centric orbits. These are not directly accreted by the planet.

But even if the ping-pong manages a direct hit on the core, all is not clear. Simulations by Agnor & Asphaug (2004); Genda et al. (2012) and others have shown that, for $v_\infty \geq 0.5v_{\text{esc}}$, the more likely outcome of a collision is "hit-and-run", where, instead of perfect accretion, the ping-pong is only partially absorbed, with much of the rest escaping as a stream of debris.

Combining these two aspects, we have the following picture for collisions in a gas-free environment. At low speeds ($v_\infty \leq 0.5v_{\text{esc}}$), the ping-pongs are predominately tidally destroyed. At higher speeds, tidal disruption is less active but ping-pong accretions are largely hit-and-run. Accretion is messy and complete clearing may take longer than our simple estimate (eq. 4). How this affects the dynamics requires a closer look.

4.4. Previous Works

It was first proposed by Chatterjee & Ford (2015) that scattering with planetesimals can repel planet pairs. They were interested in studying whether planet pairs initially trapped in MMRs can break free by scattering with the planetesimals. They reported pair repulsion – the root cause of which we elucidate here – and that the amount of repulsion scales with the mass of planetesimals.

This problem is further studied by Ghosh & Chatterjee (2023b), with the specific aim of reproducing the resonance asymmetry. Like in the current study, they initialized the period ratio of the planet pairs as a flat distribution (i.e., not only in MMRs). Within their wide belt of planetesimals, only about $1/5$ are destabilized by the planet into orbit crossing (their Fig. 2). Accounting for this inefficiency, their $m_d/m_p = 0.1$ model has an effective $\epsilon = 2\%$. For such a value, we expect an orbital repulsion of 2.2% (eq. 5), while Ghosh & Chatterjee (2023b) only found 0.3% (their Fig. A1), a repulsion efficiency that is almost one order of magnitude lower. Moreover, their simulations fail to reproduce a prominent resonance asymmetry (their Fig. 7 for 3:2 and Fig. 8 for 2:1), in contrast to our results here (Fig. 9). They do find that disks with even higher masses could produce some asymmetries, but at locations differing from that is observed.

There may be a number of factors that could help explain our differences. For instance, their simulations are expensive because they use a large number of planetesimals, so they can only perform a small number of

runs. This may introduce statistical fluctuations and obscure the asymmetry. Also, their planet sizes (based on an ad-hoc mass-radius relation) are likely larger than ours (only the core size), leading to rapid accretion. Lastly, the massive belt of ping-pongs adopted in Ghosh & Chatterjee (2023b) may exert dynamical friction on the planets, obscuring the effect of ping-pong repulsion.

Due to the failure of Ghosh & Chatterjee (2023b) to produce the MMR asymmetry, they argued that there must be a significant population of primordial resonant pairs (though only in 3:2, not in 2:1). This population does not seem warranted in our study to reproduce the asymmetry. However, there is a related conundrum on exact-resonant pairs, we address this point below.

4.5. *Caveat*

We note that currently there are a number of exoplanet pairs in libration in the 3:2 and 2:1 MMRs, mostly in systems with resonant chains (see, e.g. Dai et al. 2023). If these pairs are removed from the statistics, the region to the narrow of 3:2MMR will exhibit the expected deficit.⁶

These resonant pairs appear to be results of convergent migration, and, for some reason, have avoided the evolution outlined in this paper. The fact that they exist mainly in resonant chains may provide a clue, but one that has yet to be deciphered.

In this work, we have only considered ping-pong repulsion of an isolated planet pair. In reality, pairs are embedded in a ladder that are all jostling to repel each other. It is unclear what the outcome of this competition is.

5. CONCLUSION

The process that produces the observed asymmetry around MMRs may be the last imprint of planet formation. As so, it is an important key to unlock mysteries of planet formation.

We consider the situation where, after the *Kepler* planets were fully formed, and after the disappearance of the gaseous disks, there may still remain some planetesimals. These are then gradually cleared away by a combination of planet scatterings and accretion. We show that this naturally repels a planet pair, by of order the mass fraction in the small bodies. We elucidate the

origin of this repulsion: due to the larger phase space at high eccentricities and inclinations, the small bodies tend to diffuse to regions of larger angular momentum deficit. In other words, they absorb, fractionally, more energy than angular momentum from the planets. An originally circular planet pair can only adjust by pulling apart, with the outer body receiving a donation of energy and angular momentum from the inner one. The small body acts as the agent for this transaction. This dynamics is analogous to the spreading of an accretion disk, when its orbital energy is dissipated into heat. Given the prominence of the MMR feature, we expect this process to have occurred universally among all planet pairs, and to only become recognizable when the pair receives a MMR boost. Moreover, a planetesimal belt of order 1% of the planet mass is required to reproduce the magnitude of the resonance asymmetry.

Unlike repulsion by eccentricity-damping ('resonant repulsion'), this mechanism can excite planet eccentricities and inclinations. To account for the values of eccentricity and mutual inclinations reported by transit observations, the planetesimals should be of order Mercury in mass, with a total number that is in the single digits. We outline an evolutionary pathway to achieve such a residual planetesimal population near the end of the planet formation era.

We argue that accretion of these ping-pongs would not lead to appreciable atmospheric loss. The final accretion may be messy, involving either tidal disruptions or hit-and-run collisions. In addition, we have not yet explored how ping-pong repulsion alters the orbits of a trio (or more) of planets.

If such a story holds, we suggest that the late stage of planet formation is a time of clearing of a substantial amount of debris of lunar-to-Mercury mass planetesimals.

- 1 We are grateful to Hanno Rein for answering ques-
- 2 tions on REBOUND, and to Eugene Chiang, Sam Had-
- 3 den, Scott Tremaine for discussions. YW is funded by
- 4 the NSERC discovery grant, RM is funded by NASA
- 5 grants 80NSSC18K0397 and 80NSSC21K0593, and YL
- 6 is funded by NASA grant 80NSSC23K1262.

REFERENCES

- Agnor, C., & Asphaug, E. 2004, *ApJL*, 613, L157, doi: [10.1086/425158](https://doi.org/10.1086/425158)
- Batygin, K., & Adams, F. C. 2017, *AJ*, 153, 120, doi: [10.3847/1538-3881/153/3/120](https://doi.org/10.3847/1538-3881/153/3/120)

⁶ These resonant pairs are also absent from the low-noise TTV sample in Fig. 11, as their TTV signals are 'noisy' due to the presence of a third body.

- Batygin, K., & Morbidelli, A. 2013, *AJ*, 145, 1, doi: [10.1088/0004-6256/145/1/1](https://doi.org/10.1088/0004-6256/145/1/1)
- Boss, A. P., Cameron, A. G. W., & Benz, W. 1991, *Icarus*, 92, 165, doi: [10.1016/0019-1035\(91\)90042-R](https://doi.org/10.1016/0019-1035(91)90042-R)
- Chatterjee, S., & Ford, E. B. 2015, *ApJ*, 803, 33, doi: [10.1088/0004-637X/803/1/33](https://doi.org/10.1088/0004-637X/803/1/33)
- Choksi, N., & Chiang, E. 2022, arXiv e-prints, arXiv:2211.15701, doi: [10.48550/arXiv.2211.15701](https://doi.org/10.48550/arXiv.2211.15701)
- Dai, F., Masuda, K., Beard, C., et al. 2023, *AJ*, 165, 33, doi: [10.3847/1538-3881/aca327](https://doi.org/10.3847/1538-3881/aca327)
- Deck, K. M., & Batygin, K. 2015, *ApJ*, 810, 119, doi: [10.1088/0004-637X/810/2/119](https://doi.org/10.1088/0004-637X/810/2/119)
- Deck, K. M., Payne, M., & Holman, M. J. 2013, *ApJ*, 774, 129, doi: [10.1088/0004-637X/774/2/129](https://doi.org/10.1088/0004-637X/774/2/129)
- Fabrycky, D. C., Lissauer, J. J., Ragozzine, D., et al. 2014, *ApJ*, 790, 146, doi: [10.1088/0004-637X/790/2/146](https://doi.org/10.1088/0004-637X/790/2/146)
- Fernandez, J. A., & Ip, W. H. 1984, *Icarus*, 58, 109, doi: [10.1016/0019-1035\(84\)90101-5](https://doi.org/10.1016/0019-1035(84)90101-5)
- Genda, H., Kokubo, E., & Ida, S. 2012, *ApJ*, 744, 137, doi: [10.1088/0004-637X/744/2/137](https://doi.org/10.1088/0004-637X/744/2/137)
- Ghosh, T., & Chatterjee, S. 2023a, *MNRAS*, doi: [10.1093/mnras/stad2962](https://doi.org/10.1093/mnras/stad2962)
- . 2023b, *ApJ*, 943, 8, doi: [10.3847/1538-4357/aca58e](https://doi.org/10.3847/1538-4357/aca58e)
- Goldreich, P., & Schlichting, H. E. 2014, *AJ*, 147, 32, doi: [10.1088/0004-6256/147/2/32](https://doi.org/10.1088/0004-6256/147/2/32)
- Hadden, S., & Lithwick, Y. 2014, *ApJ*, 787, 80, doi: [10.1088/0004-637X/787/1/80](https://doi.org/10.1088/0004-637X/787/1/80)
- . 2017, *AJ*, 154, 5, doi: [10.3847/1538-3881/aa71ef](https://doi.org/10.3847/1538-3881/aa71ef)
- Hahn, J. M., & Malhotra, R. 1999, *AJ*, 117, 3041, doi: [10.1086/300891](https://doi.org/10.1086/300891)
- . 2005, *AJ*, 130, 2392, doi: [10.1086/452638](https://doi.org/10.1086/452638)
- Henrard, J., & Lemaître, A. 1983, *Celestial Mechanics*, 30, 197, doi: [10.1007/BF01234306](https://doi.org/10.1007/BF01234306)
- Henrard, J., Lemaître, A., Milani, A., & Murray, C. D. 1986, *Celestial Mechanics*, 38, 335, doi: [10.1007/BF01238924](https://doi.org/10.1007/BF01238924)
- Izidoro, A., Ogihara, M., Raymond, S. N., et al. 2017, *MNRAS*, 470, 1750, doi: [10.1093/mnras/stx1232](https://doi.org/10.1093/mnras/stx1232)
- Kokubo, E., & Ida, S. 1998, *Icarus*, 131, 171, doi: [10.1006/icar.1997.5840](https://doi.org/10.1006/icar.1997.5840)
- Laskar, J. 1997, *A&A*, 317, L75
- Lissauer, J. J., Ragozzine, D., Fabrycky, D. C., et al. 2011, *ApJS*, 197, 8, doi: [10.1088/0067-0049/197/1/8](https://doi.org/10.1088/0067-0049/197/1/8)
- Lithwick, Y., & Wu, Y. 2012, *ApJL*, 756, L11, doi: [10.1088/2041-8205/756/1/L11](https://doi.org/10.1088/2041-8205/756/1/L11)
- Lithwick, Y., Xie, J., & Wu, Y. 2012, *ApJ*, 761, 122, doi: [10.1088/0004-637X/761/2/122](https://doi.org/10.1088/0004-637X/761/2/122)
- Morrison, S. J., & Kratter, K. M. 2018, *MNRAS*, 481, 5180, doi: [10.1093/mnras/sty2657](https://doi.org/10.1093/mnras/sty2657)
- Murray, C. D., & Dermott, S. F. 2000, *Solar System Dynamics*, doi: [10.1017/CBO9781139174817](https://doi.org/10.1017/CBO9781139174817)
- Petrovich, C., Malhotra, R., & Tremaine, S. 2013, *ApJ*, 770, 24, doi: [10.1088/0004-637X/770/1/24](https://doi.org/10.1088/0004-637X/770/1/24)
- Pichierri, G., Batygin, K., & Morbidelli, A. 2019, *A&A*, 625, A7, doi: [10.1051/0004-6361/201935259](https://doi.org/10.1051/0004-6361/201935259)
- Press, W. H., Flannery, B. P., & Teukolsky, S. A. 1986, *Numerical recipes. The art of scientific computing*
- Rein, H. 2012, *MNRAS*, 427, L21, doi: [10.1111/j.1745-3933.2012.01337.x](https://doi.org/10.1111/j.1745-3933.2012.01337.x)
- Rein, H., & Liu, S. F. 2012, *A&A*, 537, A128, doi: [10.1051/0004-6361/201118085](https://doi.org/10.1051/0004-6361/201118085)
- Rein, H., & Spiegel, D. S. 2015, *MNRAS*, 446, 1424, doi: [10.1093/mnras/stu2164](https://doi.org/10.1093/mnras/stu2164)
- Sessin, W., & Ferraz-Mello, S. 1984, *Celestial Mechanics*, 32, 307, doi: [10.1007/BF01229087](https://doi.org/10.1007/BF01229087)
- Sridhar, S., & Tremaine, S. 1992, *Icarus*, 95, 86, doi: [10.1016/0019-1035\(92\)90193-B](https://doi.org/10.1016/0019-1035(92)90193-B)
- Steffen, J. H., & Hwang, J. A. 2015, *MNRAS*, 448, 1956, doi: [10.1093/mnras/stv104](https://doi.org/10.1093/mnras/stv104)
- Watanabe, S.-I., & Miyama, S. M. 1992, *ApJ*, 391, 318, doi: [10.1086/171348](https://doi.org/10.1086/171348)
- Wetherill, G. W., & Stewart, G. R. 1989, *Icarus*, 77, 330, doi: [10.1016/0019-1035\(89\)90093-6](https://doi.org/10.1016/0019-1035(89)90093-6)
- Wu, Y., & Lithwick, Y. 2013, *ApJ*, 772, 74, doi: [10.1088/0004-637X/772/1/74](https://doi.org/10.1088/0004-637X/772/1/74)
- Xie, J.-W. 2014, *ApJ*, 786, 153, doi: [10.1088/0004-637X/786/2/153](https://doi.org/10.1088/0004-637X/786/2/153)
- Yalinewich, A., & Schlichting, H. 2019, *MNRAS*, 486, 2780, doi: [10.1093/mnras/stz1049](https://doi.org/10.1093/mnras/stz1049)
- Yalinewich, A., & Schlichting, H. E. 2020, *MNRAS*, 497, 4143, doi: [10.1093/mnras/staa2139](https://doi.org/10.1093/mnras/staa2139)
- Zhu, W., Petrovich, C., Wu, Y., Dong, S., & Xie, J. 2018, *ApJ*, 860, 101, doi: [10.3847/1538-4357/aac6d5](https://doi.org/10.3847/1538-4357/aac6d5)

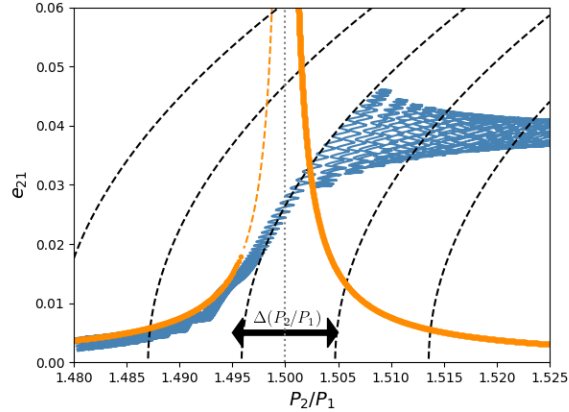


Figure 12. Repulsion associated with a MMR crossing is related to the unstable fixed-point. The horizontal axis shows P_2/P_1 and the vertical axis the relative eccentricity (a reduced variable, see text). The blue curve shows the REBOUND integration of an equal-mass planet pair, being gradually pushed apart across the 3:2MMR. The black dashed curves correspond to constant Brouwer integrals, while the orange curves are the fixed points for eccentricity, with the solid orange curve representing the stable fixed-point and the dashed curve the unstable one. As the pair gradually moves from left to right, they encounter the unstable fixed-point. Within one libration time, the pair jump across the MMR. The associated kicks in period ratio and eccentricities are discussed in the text.

APPENDIX

A. KICKS FROM A DIVERGENT ENCOUNTER WITH A MEAN MOTION RESONANCE

When two planets migrate across an MMR divergently, they acquire kicks to their eccentricities and period ratio (Henrard & Lemaître 1983; Murray & Dermott 2000). We illustrate this with a REBOUND integration. We gently push two planets apart, across the 3:2MMR, by imposing an inwards \dot{a} on the inner one. The result is the blue curve in Fig. 12, which shows the two planets’ e_{21} (the magnitude of the difference of their eccentricity vectors) versus their period ratio. The masses of the planets are each $8M_\oplus$, and they are initialized with P_2/P_1 inward of the MMR. The initial e_{21} has zero free component—i.e., it is placed at its analytic fixed point, which is traced out by the orange curve. The planets gradually evolve to larger P_2/P_1 .⁷ The kicks in e_{21} and P_2/P_1 upon resonant crossing are evident in the figure.

The behavior in Fig. 12 can be quantified by comparing with what happens for non-migrating planets. A planet pair near a MMR may be reduced to a Hamiltonian with two variables, e_{21} and ϕ , where ϕ is the resonant angle (Sessin & Ferraz-Mello 1984; Henrard et al. 1986; Deck et al. 2013). The MMR gives rise to oscillations in both e_{21} and P_2/P_1 , which are coupled via a constant of the motion, B :

$$B \approx \frac{P_2}{P_1} - \frac{3p}{2} \left(\frac{p+1}{p} \right)^{5/3} e_{21}^2, \quad (\text{A1})$$

for a $p+1 : p$ MMR. The expression in Eq. A1 follows from the conservation of Γ' in Deck & Batygin (2015), as approximated in their Eq. 3. Their approximation assumes that p is large in the Laplace coefficients, but we find nonetheless that it is adequate for the 3:2 and the 2:1. See Deck et al. (2013) for a more thorough discussion of the approximations involved. The constant B is often referred to as the “Brouwer integral” (e.g., Hahn & Malhotra 2005).

Fig. 12 shows curves of constant B near the 3:2 MMR. The resonant oscillations are visible as the motion that nearly tracks the constant B curves. As the planets are pushed apart (P_2/P_1 increases), they adiabatically follow the fixed-point solution, determined using the Hamiltonian given in Eq. 1 of Deck & Batygin (2015) for a given value of

⁷ Although the imposed $|\dot{a}|/a$ used for Fig. 12 is small relative to the resonant libration frequency, it is much larger than realistic migration values. That artificial enhancement makes the resonant librations in Fig. 12 more visible, as it prevents successive librations from overlapping too much.

B (or Γ'). However, at a certain value of P_2/P_1 (~ 1.4955 for our case), the fixed point becomes unstable. The pair jump within a single libration time to $P_2/P_1 \sim 1.505$. After that, it continues to undergo MMR-driven oscillations, but now around the other stable fixed point, with a roughly constant free eccentricity.

The kick in P_2/P_1 is of order the width of the MMR, which, for an equal-mass pair, is approximated as (Batygin & Adams 2017),

$$\Delta \left(\frac{P_2}{P_1} \right)_{\text{MMR}} \approx 5 \left[\frac{\sqrt{p+1}(M_{p1} + M_{p2})}{M_*} \right]^{2/3}, \quad (\text{A2})$$

and is $= 0.0095(M_p/8M_\oplus)^{2/3}$ for the 3:2 MMR, consistent with what is seen in the figure ($1.505-1.4955=0.0095$). For the 2:1 MMR, the kick is $0.0082(M_p/8M_\oplus)^{2/3}$, as we have also verified with REBOUND integrations.

The kick in e_{21} may be approximated as follows. From Fig. 12, we see that immediately after the blue curve crosses the unstable fixed point, it hugs a particular constant- B curve. Given the kick in $\Delta \left(\frac{P_2}{P_1} \right)_{\text{MMR}}$ along that constant- B curve, we use the constancy of B (Eq. A1) to find the corresponding kick in e_{21} , as

$$\Delta(e_{21})_{\text{MMR}} = \left(\frac{2}{3p} \left(\frac{p}{p+1} \right)^{5/3} \Delta \left(\frac{P_2}{P_1} \right)_{\text{MMR}} \right)^{1/2} \approx 1.8 \frac{p^{1/3}}{(p+1)^{2/3}} \left[\frac{M_{p1} + M_{p2}}{M_*} \right]^{1/3}. \quad (\text{A3})$$

This corresponds to the net kick, starting from $e_{21} = 0$ far from resonance. The above expression evaluates to $\Delta(e_{21})_{\text{MMR}} = 0.040(M_p/8M_\oplus)^{1/3}$ for the 3:2 MMR, consistent with the figure, and is 4% larger than that for the 2:1 MMR.